

## In-Situ X-ray Scattering Study of Continuous Silica–Surfactant Self-Assembly during Steady-State Dip Coating

Dhaval A. Doshi,<sup>†,§</sup> Alain Gibaud,<sup>‡,§</sup> Nanguo Liu,<sup>†</sup> Dietmar Sturmayer,<sup>||</sup> Anthony P. Malanoski,<sup>†</sup> Darren R. Dunphy,<sup>‡</sup> Hongji Chen,<sup>†</sup> Suresh Narayanan,<sup>⊥</sup> Andrew MacPhee,<sup>⊥,#</sup> Jin Wang,<sup>⊥</sup> Scott T. Reed,<sup>‡</sup> Alan J. Hurd,<sup>‡,§</sup> Frank van Swol,<sup>†,‡</sup> and C. Jeffrey Brinker<sup>\*,†,‡</sup>

*Department of Chemical and Nuclear Engineering and Center for Micro-Engineered Materials, University of New Mexico, Albuquerque, New Mexico, Sandia National Laboratories, Albuquerque, New Mexico, Université du Maine, Faculté des Sciences, UMR 6087, CNRS 72085, Le Mans, Cedex 09, France, Institute of Materials Chemistry, Vienna University of Technology, Vienna, Austria, and Advanced Photon Source, Argonne National Laboratory, Argonne, Illinois*

*Received: October 15, 2002; In Final Form: June 2, 2003*

Inorganic mesoporous thin-films are important for applications such as membranes, sensors, low-dielectric-constant insulators (so-called low  $\kappa$  dielectrics), and fluidic devices. Over the past five years, several research groups have demonstrated the efficacy of using evaporation accompanying conventional coating operations such as spin- and dip-coating as an efficient means of driving the self-assembly of homogeneous solutions into highly ordered, oriented, mesostructured films. Understanding such evaporation-induced self-assembly (EISA) processes is of interest for both fundamental and technological reasons. Here, we use spatially resolved 2D grazing incidence X-ray scattering in combination with optical interferometry during steady-state dip-coating of surfactant-templated silica thin-films to structurally and compositionally characterize the EISA process. We report the evolution of a hexagonal (p6 mm) thin-film mesophase from a homogeneous precursor solution and its further structural development during drying and calcination. Monte Carlo simulations of water/ethanol/surfactant bulk phase behavior are used to investigate the role of ethanol in the self-assembly process, and we propose a mechanism to explain the observed dilation in unit cell dimensions during solvent evaporation.

### Introduction

The precise control of porosity in inorganic thin-film materials is important for applications such as membranes, sensors, low-dielectric-constant insulators (so-called low  $\kappa$  dielectrics), and fluidic devices. Although “classical” sol–gel processing of xerogel films<sup>1</sup> and new low-temperature/pressure routes to aerogel films<sup>2</sup> allow control of volume fraction porosity over the range 0.2–0.9, the distribution of pore size—determined by the response of the gel to drying-induced capillary stresses—can be quite broad, especially for highly porous films.<sup>2</sup> Over the past six years, the extension of the surfactant-templating approach from mesoporous silica powders<sup>3</sup> to films<sup>4</sup> using simple evaporation-induced self-assembly (EISA) procedures<sup>5</sup> has enabled unprecedented control of pore size, orientation, and connectivity.<sup>6,7,8</sup> EISA begins with a homogeneous solution of a soluble silica (generally oligomeric oxohydroxo species we refer to as silicic acid), alcohol, water, and surfactant prepared with an initial surfactant concentration  $c_0$  much less than the critical micelle concentration (cmc) and an acid concentration (0.108 M) designed to minimize the siloxane condensation

rate.<sup>5,9</sup> Evaporation accompanying film deposition by dip-coating, spin-coating, ink-jet printing,<sup>10</sup> etc., concentrates the depositing film in surfactant and silica, inducing the self-assembly of micelles and their further organization into liquid crystalline silica/surfactant mesophases. Recent efforts to structurally and chemically characterize the EISA process include spatially resolved spectroscopic studies of molecular probes,<sup>6,11</sup> imaging ellipsometry,<sup>12</sup> and time-resolved 1D<sup>13</sup> and 2D X-ray scattering.<sup>14</sup> Grosso et al.<sup>13</sup> used in-situ 1D X-ray scattering to study mesostructure formation in thin-films during (non-steady-state) drain-coating from sols containing various CTAB concentrations that were aged for one week to promote limited siloxane condensation. Different mesophases were obtained by varying the CTAB concentration; however, the use of a 1D detector prevented a complete evaluation of the structural evolution. By comparing the in situ 1D X-ray scattering pattern (a single spot/peak) with the diffraction spots of 2D X-ray scattering patterns obtained on dried film samples, they inferred a possible 3D hexagonal-to-cubic transformation. Their recent communication<sup>14</sup> reports the use of a 2D detector to follow, in situ, the evolution of a cubic thin-film mesophase from a homogeneous solution through a lamellar intermediate. However, the drain-coating process never reaches steady-state, making it difficult to estimate the portion of the film thinning due to draining (which does not change the composition) and the portion due to evaporation (which enriches the depositing film in silica and surfactant, thus driving self-assembly). Such a transient coating procedure precludes establishment of com-

\* Author to whom correspondence should be addressed at Advanced Materials Laboratory, 1001 University SE, Albuquerque, NM 87106. Ph: 505-272-7627. Fax: 505-272-7304. E-mail: cjbrink@sandia.gov.

<sup>†</sup> University of New Mexico.

<sup>‡</sup> Sandia National Laboratories.

<sup>§</sup> Université du Maine.

<sup>||</sup> Vienna University of Technology.

<sup>⊥</sup> Argonne National Laboratory.

<sup>#</sup> Currently at University of California, Berkeley, CA.

<sup>§</sup> Currently at Los Alamos National Laboratory, NM.

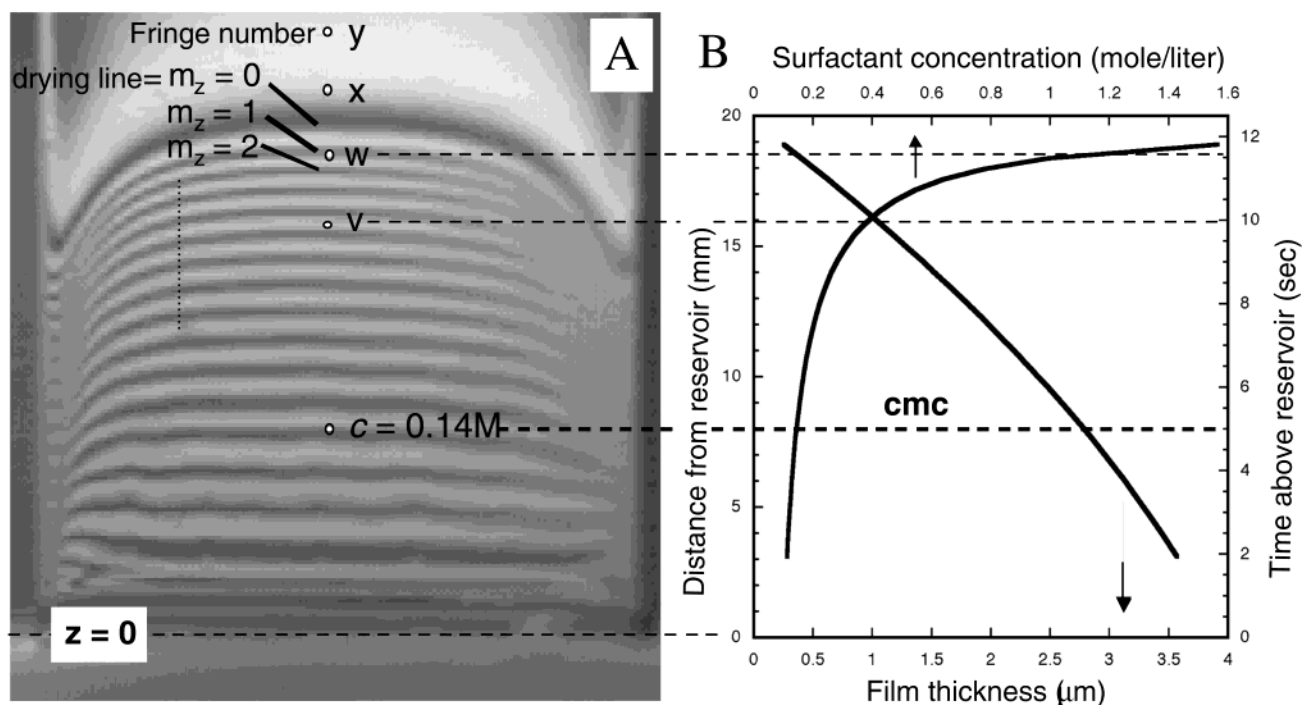


**Figure 1.** (A) Optical interference image of a steady-state film drying profile used to calculate the film profile using eq 1. (B) The calculated film thickness and surfactant concentration.

position–mesostructure relationships needed to understand and ultimately control EISA.

Here, as in our initial report employing molecular probes,<sup>6</sup> we exploit the steady-state nature of dip-coating<sup>15</sup> to spatially and temporally resolve the complete sequence of structural and compositional changes accompanying evaporation-induced self-assembly. By performing spatially resolved 2D grazing incidence small-angle X-ray scattering (GISAXS) experiments in combination with optical interferometry,<sup>2,6,11</sup> we characterized the evolution of a hexagonal ( $p6$  mm) thin-film mesophase from a homogeneous precursor solution and its further structural development during drying and calcination. The steady-state process allows us to observe subtle changes in the mesostructure, not observed in previous studies.<sup>13,14</sup> Monte Carlo simulations of the water/ethanol/surfactant three-phase behavior were performed to investigate the role of the changing ethanol composition in influencing self-assembly.

### Experimental Section

Precursor solutions were prepared using a two-step procedure reported previously.<sup>6</sup> Final reactant mole ratios were 1TEOS:20  $C_2H_5OH$ :5.1  $H_2O$ :0.0026  $HCl$ :0.16  $C_{16}TAB$  (cetyltrimethylammonium bromide). The effective initial solution pH ( $-\log [H_3O^+]$ ) was  $\sim 2$ , which largely precludes further siloxane condensation reactions accompanying EISA (as monitored by cantilever beam bending measurements<sup>16</sup>), thereby avoiding premature solidification/gelation and enabling self-assembly to proceed unimpeded. The 300  $\mu m$ -thick Si(100) substrates were dip-coated at a withdrawal rate of 1.6 mm/s at 25 °C and 9% relative humidity.

X-ray experiments were performed at the SRI-CAT's 1-BM-C beamline of the Advanced Photon Source, Argonne National Laboratory. In the experiment, an 11 keV X-ray beam was focused to a  $0.5 \times 0.5$  mm<sup>2</sup> spot on the silicon substrate at an incident angle of 0.35°. X-ray scattering patterns were collected on a 2D detector (image plate) positioned at a distance of 103 cm from the sample with typical imaging times of 20 s. Use of

a divergent focused beam is advantageous when recording scattering patterns with the sample at a fixed angle since it thickens the Ewald sphere. Image plate patterns were optically scanned in steps of 0.2 mm, yielding a  $2\theta$  resolution of 0.2 mrad.

### Results and Discussion

Figure 1A shows the optical interference image of a steady-state film thickness profile during dip-coating and the positions of sample volumes probed by GISAXS. The thickness profile  $h(z)$  is calculated using eq 1:

$$h(z) = \frac{(2m(z) + 1)\lambda}{4(n(z)^2 - \sin^2 \theta)^{1/2}}$$

and is plotted in Figure 1B, along with the calculated surfactant concentration,  $c$ , as a function of distance,  $z$ , and time above the sol reservoir surface: (all variables defined in ref 17). Knowing  $h(z)$ , the initial surfactant concentration,  $c(0)$ , and the initial thickness,  $h(0)$ , we calculated the  $z$ -dependent surfactant concentration  $c(z)$  from the appropriate mass balance for a nonvolatile component  $c(0) \cdot h(0) = c(z) \cdot h(z)$ , the varying surfactant concentration,  $c(z)$  is also plotted in Figure 1B.

From the reservoir surface ( $z = 0$ ) to position “ $v$ ” in Figure 1A, the GISAXS pattern shows no diffraction spots, indicating the absence of any periodic mesostructure or any incipient organization at the solid–liquid or liquid–vapor interfaces. Scattering from micelles expected to form at  $cmc = 0.14$  M (previously established by a molecular probe experiment<sup>18</sup>) cannot be discerned from the background scattering.

At position “ $v$ ” in Figure 1a (surfactant concentration  $c_v = 0.4$  M), a single Bragg spot is visible in the direction normal to the film surface with  $q_z = 0.171 \text{ \AA}^{-1}$ , corresponding to a  $d$ -spacing of 3.65 nm. At position “ $w$ ” ( $c_w = 0.8$  M), this spot is observed at a  $d$ -spacing of 3.73 nm (Figure 2A). No specular ridge (for example, a dark line joining the beam stop to the first specular Bragg reflection in Figure 2B) is seen, and diffuse

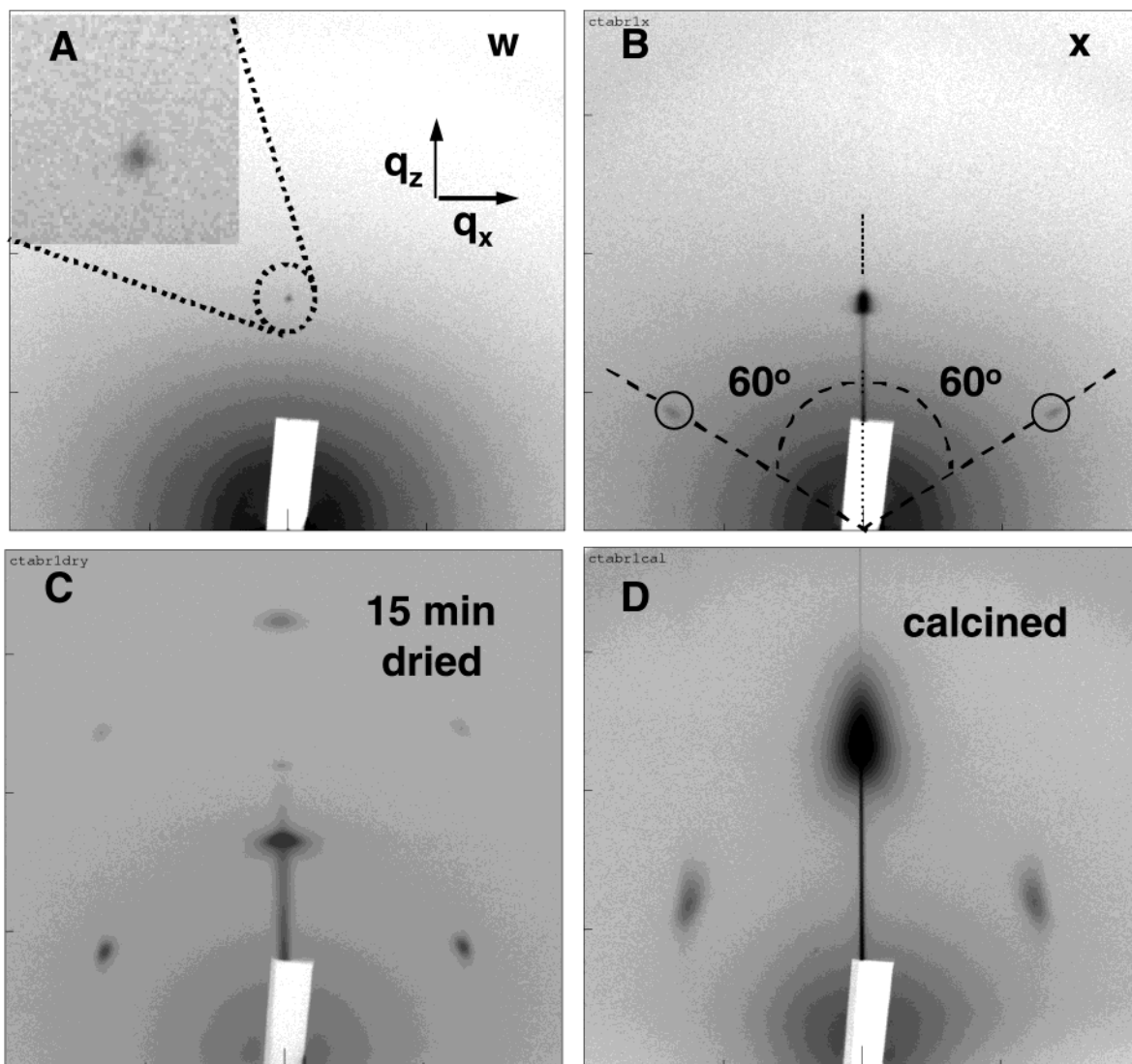


**Figure 2.** GISAXS images of mesostructured films. In-situ image from a scattering volume (A) below the drying line at position “w”. (B) just above the drying line at position “x”. (C) Film after 15 min of drying. (D) Calcined film. Images are  $0.4 \text{ \AA}^{-1}$  ( $q_z$ )  $\times$   $0.4 \text{ \AA}^{-1}$  ( $q_x$ ).

small-angle scattering is observed. The single Bragg spot is consistent with the formation of a lamellar mesophase, presumably at the liquid–vapor interface. Presence of the diffuse small angle scattering, which prevents observation of the specular ridge, suggests additional scattering from randomly positioned micelles. Due to the absence of any periodic 2D structure parallel to the substrate surface, the film at “w” can be envisioned as a mixture of 1D lamellar domains at the liquid–vapor (and perhaps liquid–solid) interfaces and a disordered micellar or wormlike mesostructure in between.

Just above the drying line ( $m_z = 0$ ), at position “x” in Figure 1A ( $c_x > 1.6 \text{ M}$ ) the GISAXS pattern is composed of Bragg spots that lie on a circle, organized  $60^\circ$  apart (see Figure 2B). The narrow specular ridge shows that the surface of the film is flat and parallel to the substrate surface. The width of the specular ridge in the off-specular direction allows determination of the instrument resolution,<sup>19</sup> which is better than  $0.0001 \text{ \AA}^{-1}$  at  $q_z = 0.1 \text{ \AA}^{-1}$ . The 6-fold symmetry of the Bragg spots indicates a highly ordered film having true hexagonal symmetry,<sup>20</sup> with tubule axes oriented parallel to the substrate surface. The hexagonal packing ( $a_{\text{hex}} = 4.43 \text{ nm}$ ) of the tubules can be described by a face-centered rectangular cell with lattice parameters  $a_{\text{fer}} = 4.43 \text{ nm}$  and  $c_{\text{fer}} = 7.65 \text{ nm}$  as shown in Figure 3A. The same symmetry is also observed 3 mm above the drying

line at position “y” in Figure 1A with an increase in the unit cell dimension,  $a_{\text{hex}} = a_{\text{fer}} = 4.6 \text{ nm}$  and  $c_{\text{fer}} = 7.94 \text{ nm}$ . This 3.8% expansion in the linear dimensions of the unit cell is attributed to an increase in the cylindrical micelle diameter.<sup>21</sup> It is known that siloxane condensation can cause restructuring of surfactant molecules, resulting in phase transformations from lamellar to hexagonal<sup>22</sup> and hexagonal to cubic,<sup>8</sup> to maintain charge-density matching at the surfactant–silica interface.<sup>8,22,23</sup> However, the optimization of the system to inhibit the siloxane condensation during the EISA process suggests other mechanisms such as ethanol loss-driven micelle expansion to be more likely candidates as we discuss later.

To investigate the role of ethanol in the self-assembly process we performed lattice Monte Carlo simulations of mixtures of water, ethanol, and surfactant. This approach strikes a good balance between molecular detail and the ability to routinely witness spontaneous self-assembly processes on an acceptable computational time scale.<sup>24</sup> The particular implementation here represents the small molecules as a simple lattice gas, single beads occupying single sites. Our surfactants are linear chains ( $\text{H}_2\text{T}_6$ ) of 2 headgroup beads and 6 tail group beads, together occupying 8 sites. The various pair-interaction strengths were chosen to best represent the known binary interactions. Briefly, the water and ethanol interaction potentials were determined

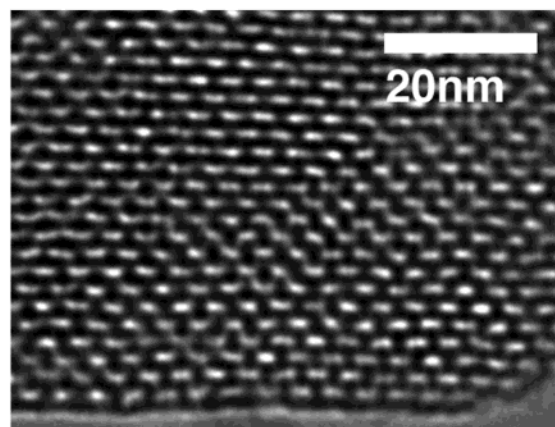
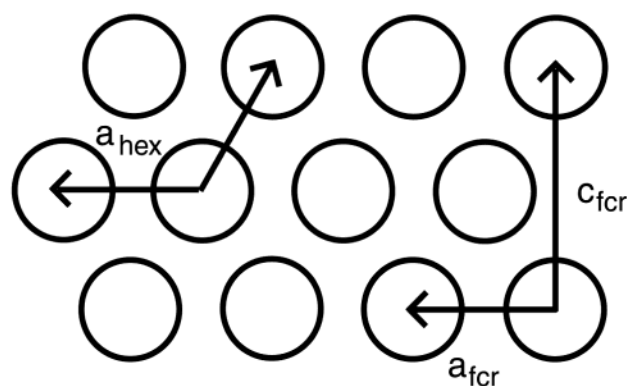


**Figure 3.** Schematic of a hexagonal unit cell shown to be equivalent to a face-centered rectangular unit cell. (B) TEM image of a calcined film showing a brick-like pattern resulting from the shrinkage of a hexagonally ordered film in the thickness direction.

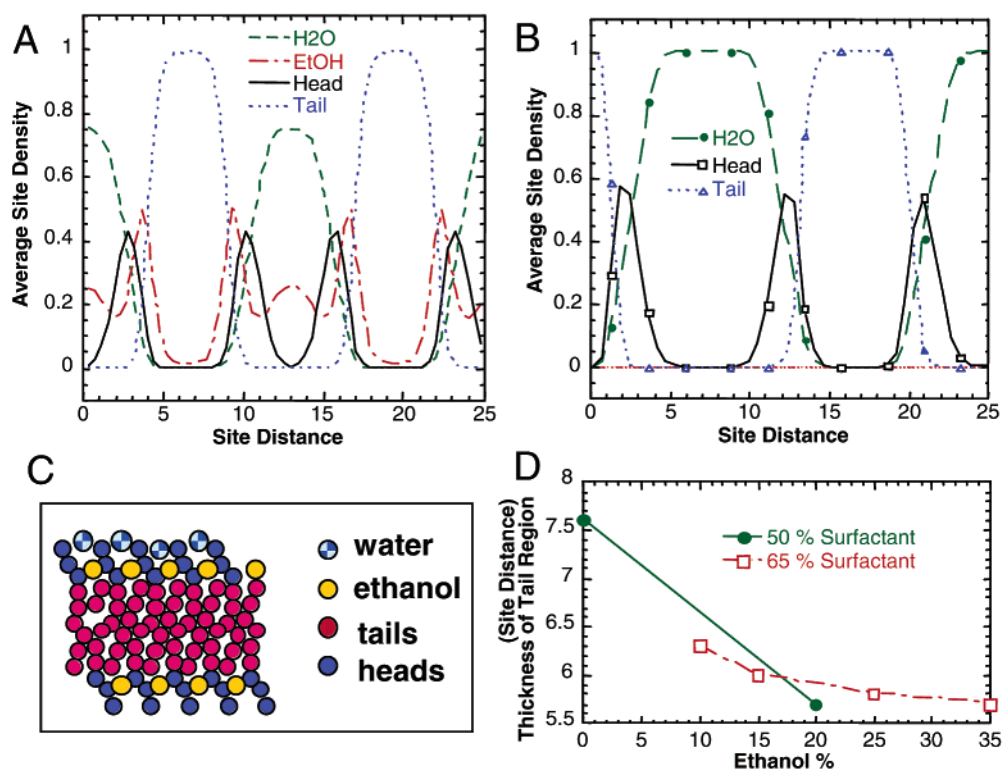


**Figure 4.** Monte Carlo simulations of a lamellar phase. (A) Average site density profiles for components in a 50%  $\text{H}_2\text{T}_6$ , 20% EtOH, 30% water system. (B) average site density profiles for components in a 50%  $\text{H}_2\text{T}_6$ , 50% water system. (C) Schematic representation of a lamellar bilayer based on MC simulations. (D) Plot of thickness of tail regions in the bilayer for different ethanol and surfactant concentrations.

from the bulk phase diagram. The self-interaction strength was determined from the critical temperatures and the ethanol–water cross-interaction was set to 4% less than the Berthelot mixing rule<sup>25</sup> to capture the two-component ethanol–water phase behavior. The water–head interaction is identical to water–water and the water–tail interaction is considered to be zero. Ethanol does not discriminate between head and tail beads, and its interaction strength is 70% of that of water–head. Previously, we mapped out the phase diagram for this model mixture and hence know that both hexagonal and lamellar phases form.<sup>26</sup> One might expect ethanol and water to behave rather similarly, so the ethanol–water mixture could be considered a single fluid phase. In such an interpretation ethanol would be merely a spectator to the self-assembly.

However, the simulations demonstrate ethanol to be a participant, actively shielding the tail sites from water (Figure 4C). Thus, there is a significant positive adsorption of ethanol

at the surfactant/water interface. The ethanol has a peak density between the head and tails, promoting significant interdigitation of head and tail groups (see Figure 4A and B). A decrease in the ethanol content of the solvent results in an unfavorable interaction between the tails and water-rich solvent, causing the bilayer spacing to increase (extent of inter-digitation decreases) as seen from the average site density profiles in Figure 4A and B. Figure 4D demonstrates the monotonic decrease in the extent of interdigitation, measured by the thickness of the tail region in the bilayer, with decreasing ethanol concentration. These results are consistent with the observed increase in the lamellar  $d$  spacing between position “ $v$ ” and “ $w$ ”.

A plausible mechanism for the observed expansion in the hexagonal mesophase is depicted in Figure 5, preferential evaporation of ethanol enriches the solvent in water increasing the solvent–hydrocarbon interfacial energy. This in turn causes stretching and reorientation of the hydrocarbon tails to minimize

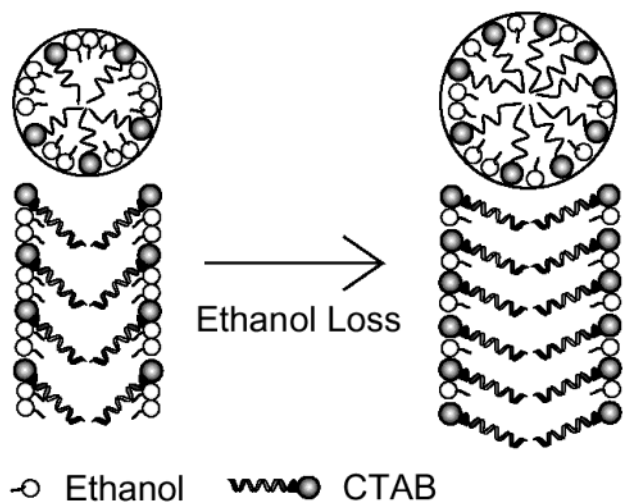


**Figure 5.** Schematic of ethanol loss driven micelle dilation. The hydrocarbon chains are shown in the trans configuration for clarity.

their contact area with the solvent, increasing the cylindrical micelle diameter and requiring an increase in the aggregation number per unit length of the cylinder and correspondingly a reduction in the effective headgroup area per surfactant molecule. Scattering experiments performed on this surfactant system in humid conditions (25% RH) have shown the extent of such an ethanol loss-driven expansion to be as large as 23%, which can be explained on the basis of higher water content in the films. Fontell et al.<sup>27</sup> report a 36% increase in the unit cell dimension (that corresponds to a 23% increase in the cylindrical micelle diameter) with decreasing ethanol content in the bulk CTAB/ethanol/water system.

The GISAXS pattern of the film after 15 min of drying (Figure 2C) reveals a distortion of the hexagonal symmetry.<sup>28</sup>  $a_{\text{fer}}$  increases to 4.83-nm, while  $c_{\text{fer}}$  reduces to 7.45 nm, and the  $02_{\text{fer}}$  Bragg spot spreads out along the off-specular direction, with planes tilting as much as  $3^\circ$  with respect to the substrate. The increase in  $a_{\text{fer}}$  is attributed to further interfacially-driven expansion of the unit cell to a point where  $a_{\text{fer}} = 4.83$  nm and  $c_{\text{fer, calculated}} = 8.36$  nm. Thereafter, the in-plane structure becomes “locked-in” by covalent attachment to the substrate, and the onset of siloxane condensation reactions causes 1-dimensional shrinkage normal to the substrate surface. Upon rotating the sample by  $90^\circ$  about the normal to the film surface, the scattering pattern remained unchanged. This indicates that the hexagonally packed tubules are incorporated into randomly oriented domains consistent with previous TEM micrographs showing swirling patterns of disclinations.<sup>6</sup>

Finally, we investigated the further development of the mesostructure during calcination to remove the surfactant templates. The sample was first heated to  $150^\circ\text{C}$  (at  $10^\circ\text{C}/\text{min}$  and maintained for 15 min) and then to  $450^\circ\text{C}$  (at  $10^\circ\text{C}/\text{min}$  and maintained for 1 h). The diffraction pattern (Figure 2D) indicates considerable shrinkage in the direction normal to the substrate surface. The  $02_{\text{fer}}$  Bragg spot shows an elongated tulip shape, indicating a distribution of unit cell dimensions ( $4.85\text{ nm} < c_{\text{fer}} < 5.83\text{ nm}$ ). The average value of  $c_{\text{fer}}$  is 5.19 nm, while the in-plane dimension  $a_{\text{fer}}$  is 4.94 nm. These values show that the in-plane structure of the film is preserved during calcination, while an average 32% shrinkage takes place in the direction normal to the surface. The corresponding TEM cross-section (Figure 3B) reveals a brick-work pattern, as expected from constrained 1D shrinkage of the parent hexagonal structure in the direction normal to the substrate surface.

## Conclusions

The results obtained in this work have provided some new chemical and structural insights into evaporation-induced self-assembly. During most of the EISA process, there is no evidence of periodic ordering—consistent with expectations from the bulk (ethanol–water–surfactant) phase diagram. Unexpected is the formation of a lamellar phase oriented parallel to the substrate. This phase, which, on the basis of its orientation, must be located at an interface, may serve to nucleate/orient the development of the ensuing hexagonal mesophase. The in-plane isotropic nature of this intermediate lamellar phase explains the lack of alignment of the hexagonal tubules along the dip-coating direction. Even if the hexagonal tubules were to be aligned in the coating direction during dip-coating, the disappearance of the aligning shear field beyond the drying line may allow the tubules to reorient randomly, giving rise to swirling patterns. Condensing the siloxane framework via vapor phase or optically generated acid catalyst<sup>8</sup> may allow such an alignment to be frozen in the final film. Progressive depletion of ethanol and enrichment of water and finally silicic acid substantially alter the mesophase as reflected by the variations in the unit cell dimensions. Monte Carlo simulations highlight the subtle effects of solvent composition on the surfactant aggregates. The ability of the depositing film to undergo continual structural transformations or alterations in response to the changing chemical composition emphasizes that, unlike traditional sol–gel thin-film formation, gelation/solidification is postponed until after completion of drying. Under acidic conditions, silanol moieties interact with hydrophilic surfactant headgroups dramatically reducing the siloxane condensation rate as confirmed by cantilever beam-bending experiments.<sup>16</sup> This allows self-assembly to proceed unimpeded, which is crucial to ensuring high-fidelity templating<sup>29</sup> and to the elaboration of EISA in other forms such as aerosol processing and ink-jet printing.<sup>30</sup>

**Acknowledgment.** This work was partially supported by the UNM/NSF Center for Micro-Engineered Materials, the French ACI “Nanostructure” under Project N° 03-01, the DOE Basic Energy Sciences Program NSET Grant DE-FG03-02ER15368, SNL’s Laboratory Directed R&D program, the U.S. Air Force Office of Scientific Research Grant F49620-01-1-0168, and Multi University Research Initiative Grant GG10306-113743/F49602-01-1-0352. Use of the Advanced Photon Source was supported by the U.S. Department of Energy, Basic Energy Sciences, Office of Science, under Contract No. W-31-109-Eng-38. This work was done partially under contract from the U.S. Department of Energy. Sandia is a multiprogram laboratory operated by Sandia Corporation, a Lockheed Martin Company, for the U.S. Department of Energy under Contract DE-AC04-94AL85000.

## References and Notes

- Brinker, C. J.; Scherer, G. W. *Sol–Gel Science: The Physics and Chemistry of Sol–Gel Processing*; Academic Press: New York, 1990.
- Prakash, S. S.; Brinker, C. J.; Hurd, A. J.; Rao, S. M. *Nature* **1995**, *374*, 439–443.
- Kresge, C. T.; Leonowicz, M. E.; Roth, W. J.; Vartuli, J. C.; Beck, J. S. *Nature* **1992**, *359*, 710–712.
- Yang, H.; Kuperman, A.; Coombs, N.; MamicheAfara S.; Ozin, G. A. *Nature* **1996**, *379*, 703–705. Aksay, I. A.; Trau, M.; Manne, S.; Honma, I.; Yao, N.; Zhou, L.; Fenter, P.; Eisenberger, P. M.; Gruner, S. M. *Science* **1996**, *273*, 892–898.
- Brinker, C. J.; Lu, Y. F.; Sellinger, A.; Fan, H. Y. *Adv. Mater.* **1999**, *11*, 579–585.
- Lu, Y. F.; Ganguli, R.; Drewien, C. A.; Anderson, M. T.; Brinker, C. J.; Gong, W. L.; Guo, Y. X.; Soyez, H.; Dunn, B.; Huang, M. H.; Zink, J. I. *Nature* **1997**, *389*, 364–368.

- (7) Ogawa, M. *Chem. Commun.* **1996**, 1149–1150. Zhao, D.; Yang, P.; Melosh, N.; Feng, J.; Chmelka, B. F.; Stucky, G. D. *Adv. Mater.* **1998**, *10*, 1380–1385. Zhao, D. Y.; Yang, P. D.; Margolese, D. I.; Chmelka, B. F.; Stucky, G. D. *Chem. Commun.* **1998**, 2499–2500. Grosso, D.; Balkenende, A. R.; Albouy, P. A.; Lavergne, M.; Mazerolles, L.; Babonneau, F. *J. Mater. Chem.* **2000**, *10*, 2085–2089. Ogawa, M.; Masukawa, N. *Microporous Mesoporous Mater.* **2000**, *38*, 35–41. Sophie, B. A.; Gacoin, T.; Jacquiod, C.; Ricolleau, C.; Babonneau, D.; Boilot, J. P. *J. Mater. Chem.* **2000**, *10*, 1331–1336.
- (8) Doshi, D. A.; Huesing, N. K.; Lu, M. C.; Fan, H. Y.; Lu, Y. F.; Simmons-Potter, K.; Potter, B. G.; Hurd, A. J.; Brinker, C. J. *Science* **2000**, *290*, 107–111.
- (9) Sehgal, R. Preparation and characterization of ultrathin sol-gel derived silica membranes for gas separation. M.S. Thesis, University of New Mexico, 1993.
- (10) Fan, H. Y.; Lu, Y. F.; Stump, A.; Reed, S. T.; Baer, T.; Schunk, R.; PerezLuna, V.; Lopez, G. P.; Brinker, C. J. *Nature* **2000**, *405*, 56–60.
- (11) Huang, M. H.; Dunn, B. S.; Soyez, H.; Zink, J. I. *Langmuir* **1998**, *14*, 7331–7333. Huang, M. H.; Dunn, B. S.; Zink, J. I. *J. Am. Chem. Soc.* **2000**, *122*, 3739–3745.
- (12) Ganguli, R. Mesoporous thin silica films created by the templating of CTAB mesophases. Master's Thesis, University of New Mexico, 1997. N. Liu unpublished.
- (13) Grosso, D.; Albouy, P. A.; Amenitsch, H.; Balkenende, A. R.; Babonneau, F. *Time-resolved in-situ X-ray diffraction study of the formation of 3D-hexagonal mesoporous silica films*; MRS: San Francisco, CA, 2000; Vol. 628. Grosso, D.; Babonneau, F.; Albouy, P. A.; Amenitsch, H.; Balkenende, A. R.; Brunet-Bruneau, A.; Rivory, J. *Chem. Mater.* **2002**, *14*, 931–939.
- (14) Grosso, D.; Balkenende, A. R.; Albouy, P. A.; Ayrál, A.; Amenitsch, H.; Babonneau, F. *Chem. Mater.* **2001**, *13*, 1848–1856. Grosso, D.; Babonneau, F.; Soler-Illia, G.; Albouy, P. A.; Amenitsch, H. *Chem. Commun.* **2002**, 748–749.
- (15) Brinker, C. J.; Hurd, A. J. *J. Phys. III* **1994**, *4*, 1231–1242.
- (16) Samuel, J.; Brinker, C. J.; Frink, L. J. D.; van Swol, F. *Langmuir* **1998**, *14*, 2602–2605. Lu, M. Drying and calcination of sol-gel coatings. Ph.D. Dissertation, University of New Mexico, 2001. Lu, M.; Brinker, C. J. *Stress Development in Low Dielectric Constant Silica Films during Drying and Heating Process*; Materials Research Society (MRS): Boston, MA, 1999; Vol. 594.
- (17)  $\lambda = 546$  nm,  $\theta = 65^\circ$ , the refractive index  $n(z)$ , varies from 1.37 (sol) to 1.46 (film),  $m_z = 1$  for first dark fringe below the drying line ( $m_z = 0$ ).
- (18) From Lu. et al.<sup>6</sup> CTAB cmc = 0.14 M,  $z(\text{cmc}) = 8$  mm. Estimated position based on same ethanol concentrated,  $z(\text{cmc}) = 9.4$  mm.
- (19) Gibaud, A.; Vignaud, G.; Sinha, S. K. *Acta Crystallogr., Sect. A—Fundamentals of Crystallography* **1993**, *49*, 642–648.
- (20) The lattice parameter along the third direction was not accessible, attempts of conducting the experiment in transmission geometry were inconclusive due to low signal-to-noise ratios, and post coating analysis shows absence of a 3D structure.
- (21) Doshi, D. A. Understanding and Directing Self-Assembly of Inorganic Nanostructures. Ph.D. Dissertation, University of New Mexico, 2002.
- (22) Monnier, A.; Schuth, F.; Huo, Q.; Kumar, D.; Margolese, D.; Maxwell, R. S.; Stucky, G. D.; Krishnamurthy, M.; Petroff, P.; Firouzi, A.; Janicke, M.; Chmelka, B. F. *Science* **1993**, *261*, 1299–1303.
- (23) Tolbert, S. H.; Landry, C. C.; Stucky, G. D.; Chmelka, B. F.; Norby, P.; Hanson, J. C.; Monnier, A. *Chem. Mater.* **2001**, *13*, 2247–2256.
- (24) Rankin, S. E.; Malanoski, A. P.; van Swol, F. *Monte Carlo Simulation of Amphiphile Self-Assembly during Dip Coating*; MRS: Boston, MA, 2001; Vol. 636.
- (25) Hansen, J.-P.; McDonald, I. R. *Theory of Simple Liquids*, 2nd ed.; Academic Press: London, England, 1986.
- (26) Sturmayer, D.; Bauer, J.; Launay, B.; Kickelbick, G.; Huesing N.; Malanoski, A. P.; Doshi, D. A.; van Swol, F. B. PDMS–PEO Block Copolymers as Surfactants in the Synthesis of Mesoporous Silica: A Theoretical and Practical Approach, (submitted).
- (27) Fontell, K.; Khan, B.; Lindstrom, D.; Maciejewska, D.; Puang-Ngern, S. *Colloid Polym. Sci.* **1991**, *269*, 727–742.
- (28) Klotz, M.; Albouy, P. A.; Ayrál, A.; Menager, C.; Grosso, D.; VanderLee, A.; Cabuil, V.; Babonneau, F.; Guizard, C. *Chem. Mater.* **2000**, *12*, 1721–1728.
- (29) Raman, N. K.; Anderson, M. T.; Brinker, C. J. *Chem. Mater.* **1996**, *8*, 1682–1701.
- (30) Lu, Y.; Fan, H.; Stump, A.; Ward, T. L.; Rieker, T.; Brinker, C. J. *Nature* **1999**, *398*, 223–226.